Chemical Engineering Journal 429 (2022) 132128

Contents lists available at ScienceDirect

Chemical Engineering Journal

journal homepage: www.elsevier.com/locate/cej

Confined Pd clusters with dynamic structure for highly efficient Cascade-type catalysis

Xiao-Chen Ma [a], Chun Pu [a], Yue-Xing Zhang [b], Gang-Gang Chang [a,*], Ge Tian [a], Si-Ming Wu [a], Jia-Wen Liu [a], Zhi-Yi Hu [a], Li-Ying Wang [c], Yi-Xia Yin [a], Christoph Janiak [d], Xiao-Yu Yang [a,e,f,*]

[a] State Key Laboratory of Advanced Technology for Materials Synthesis and Processing &School of Chemistry, Chemical Engineering and Life Science & School of Materials Science and Engineering, Wuhan University of Technology, Wuhan, Hubei, 430070, China
[b] Hubei Collaborative Innovation Center for Advanced Organic Chemical Materials, Ministry of Education Key Laboratory for the Synthesis and Application of Organic Functional Molecules, College of Chemistry and Chemical Engineering, Hubei University, Wuhan, Hubei, 430062, China
[c] State Key Laboratory of Magnetic Resonance and Atomic and Molecular Physics, Wuhan Institute of Physics and Mathematics, The Chinese Academy of Sciences, Wuhan, Hubei, 430071, China
[d] Electron Microscopy for Materials Science (EMAT), University of Antwerp, Groenenborgerlaan 171, Antwerpen, B-2020 Belgium
[e] Qingdao National Laboratory for Marine Science and Technology, Qingdao, 266237, China
[f] School of Engineering and Applied Sciences, Harvard University, Cambridge, MA 02138, USA

ARTICLE INFO

Keywords:
Confined Pd clusters
Dynamic nanostructure
Cascade-type catalysis
Regenerable catalysts
Directed transformation

ABSTRACT

Efficient regeneration of Pd catalysts is a challenge and has a very high technological importance. Herein, we report confined Pd clusters with the ultrafine size (1.2 nm) and ultralow loading amount (0.14 wt%) in a metal–organic framework (MOF), which could potentially allow for the successive realization of the cascade-type catalytic reaction from starting reagents to final desired products, and thus to avoid the excessive processes, save energy and reduce waste. Experiments and theoretical computations have been conducted to study the strong host–guest interaction between the Pd clusters and the MOF support, leading to the high catalytic activity and dynamic of the Pd clusters. A unique dynamic structure from active disordered arrangement to deactive crystalline arrangement and then back to the active disordered arrangement (>99% of activity after regeneration by simple H_2 reduction). The MOF-confined Pd shows excellent catalytic activity (>99% activity), selectivity (around 100%) and stability (>99% activity after recycling) under mild reaction conditions (atmospheric temperature and pressure).

1. Introduction

Palladium (Pd) metal is one of the most used general homo- and heterogenous redox catalysts and is typically regarded as the most efficient catalyst for hydrogenation reactions [1-7]. The fine balance of excellent hydrogen activation through homolytic H_2 cleavage, efficient substrate binding through coordination of unsaturated bonds and/or easy oxidative addition/reductive elimination often gives an advantage to the Pd catalyst compared to its competitors, primarily represented by other platinum-group metals [8-14]. A number of approaches for the optimization of heterogenous Pd catalysts exist and are actively pursued, for example, by tuning the nature and morphology of the catalytic supports, the size and crystallinity of the immobilized particles and the use of promotor species [15-19]. The evolution of the catalyst state during the reaction often leads to a decrease of the catalyst efficiency and ultimately to its deactivation. The high surface energy of the active catalytic sites is lost due to poisoning, local structural transformations as well as aggregation associated with the migration of the surface-bound species [20-25]. For a number of catalysts, the regeneration does not pose serious problems, particularly when only the substrate diffusion is hindered (e.g. coking of zeolites, with regeneration by calcination) [26-29]. Straightforward regeneration of nanoparticulated catalytic species is generally not feasible due to dynamic transformations (e.g. aggregation of Nanoparticles (NPs)). Efficient regeneration of heterogenous catalysts with ultra-fine dispersed active components is an interesting scientific problem, which also has a very high technological importance [30-33].

Cascade-type catalytic reaction processes incorporate several

* Corresponding authors at: State Key Laboratory of Advanced Technology for Materials Synthesis and Processing &School of Chemistry, Chemical Engineering and Life Science & School of Materials Science and Engineering, Wuhan University of Technology, Wuhan, Hubei, 430070, China Xiao-Yu Yang.
E-mail addresses: changgang2016@whut.edu.cn (G.-G. Chang), xyyang@seas.harvard.edu (X.-Y. Yang).

https://doi.org/10.1016/j.cej.2021.132128
Received 27 April 2021; Received in revised form 24 August 2021; Accepted 26 August 2021
Available online 11 September 2021
1385-8947/

reactions to produce a final product in one operation. Its advantages are evident: reduction of the number of steps involved in a chemical conversion, thus a reduction of energy consumption, less waste products, enhanced performances and increased operational safety [34]. Confinement of noble nanometals in a pore matrix is a promising way to special types of catalysts and the beauty of the confined noble metals lies in their unique confinement effects for a significant enhancement of the catalytic activity [35-38]. MOF-confined Pd catalysts, having periodic nano-architectures, well-defined Pd nanostructures, and controlled acid/base functions, could potentially allow for the successive realization of cascade-type catalytic reaction and to realize right and efficient functionality. However, dynamic transformations are still rare, and the dynamic aggregation mostly restricted to pore-confined NPs [39]. When NPs are not strictly confined, the mobility of the catalytic species makes the control over the crystallinity, size and morphology of the NPs even more problematic.

In this contribution, we report the formation of Pd clusters in MOF-253 (Pd@MOF-253), which was applied to the Knoevenagel condensation-hydrogenation reaction. The target product (benzylmalononitrile) was an important intermediate for the production of α, β-unsaturated carbonyl compounds, pharmaceutical, fine chemicals and agrochemical industries [18]. Particularly, the chelating bipyridine linkers of the Pd@MOF-253 support can prevent aggregation of the immobilized Pd clusters and exercise dynamic control over their crystallinity. A plausible mechanism of the dynamic particle transformation is proposed based on our experimental data and theoretical calculations.

2. Materials and methods

2.1. Materials

Aluminum chloride hexahydrate (Macklin, 99%), 2,2′-bipyridine-5,5′-dicarboxylic acid (H_2bpydc, Ark Pharm, 97%), 4,4′-biphenyldicarboxylic acid (H_2bpdc, Aladdin Industrial Co., China, 97%), palladium acetate (Ark Pharm, 98%), benzaldehyde (Adamas-beta, 99%), malonitrile (Aladdin Industrial Co., China, 99%) were obtained as indicated and used without further purification. Various substituted benzaldehydes used in this study were analytical grade with purity higher than 98%. All the other chemicals (AR grade) were commercially available and used without further purification.

2.2. Synthesis of MOF-253

The MOF was synthesized and purified according to a previously reported method [40]. For MOF-253, typically, a mixture of $AlCl_3{\cdot}6H_2O$ (151 mg, 0.625 mmol) and H_2bpydc (153 mg, 0.625 mmol) in 10 mL of N, N'-dimethylformamide (DMF) was placed in 25 mL of a Teflon-capped scintillation vial, then heated at 120 °C for 24 h, and cooled to room temperature. The resulting white microcrystalline powder was filtered and washed with DMF. Further, the product was purified with methanol via a soxhlet extraction for 24 h, after which the powder was collected by filtration and vacuum dried at 80 °C for 12 h.

2.3. Synthesis of DUT-5

In a typical synthesis, 4,4′-biphenyldicarboxylic acid (H_2bpdc) (0.26 g) and $Al(NO_3)_3{\cdot}9H_2O$ (0.52 g) was separately dissolved in 30 cm^3 DMF, and the mixture was filled in a 100 cm^3 Teflon liner, placed in an autoclave, heated to 120 °C for 24 h and then cooled to room temperature. After the product was separated by centrifugation, the sediment was washed with DMF and EtOH for three times. The product was collected by filtration and vacuum dried at 80 °C for 12 h.

2.4. Synthesis of × Pd@MOF-253 (x stands for the loading amount of Pd species)

The fabrication of Pd active sites in MOF-253 with various loading amounts was realized by using a simple impregnation method and then reduction in H_2 atmosphere. Specifically, the mixture of $Pd(OAc)_2$ and MOF-253 in toluene was stirred at room temperature overnight. After that, the solid was filtered, adequately washed with excess toluene and acetone, and dried under vacuum to afford the $Pd(OAc)_2$@MOF-253. The reduction process of the precursor loaded $Pd(OAc)_2$@MOF-253 was performed under a 50 mL/min flow of 10% H_2/Ar at 200 °C for 3 h. ICP-OES results reveal that the Pd loading amount in Pd@MOF-253 was 0.14 wt%, 0.23 wt% and 0.27 wt%, respectively. For comparison, the same method was also applied to the synthesis of Pd@DUT-5.

2.5. Catalytic Knoevenagel condensation-hydrogenation reaction

The one-pot tandem Knoevenagel condensation-hydrogenation reactions were carried out in a 25 mL stainless-steel autoclave with magnetic stirrer. In a typical procedure, benzaldehyde (0.4 mmol) and malononitrile (1.2 mmol) were dispersed into toluene (6 mL), followed by adding catalysts. Next, the obtained solution was magnetically stirred at 600 rpm in a stainless-steel autoclave at room temperature for a period of time to finish the Knoevenagel condensation of benzaldehyde and malononitrile. Subsequently, the autoclave was purged with H_2 for 10 times, and the H_2 pressure of the autoclave was set at 0.12 MPa for the subsequent hydrogenation process. The reaction solution was magnetically stirred at room temperature for designated time. After the reaction was finished, the conversion and the selectivity of products were analyzed by gas chromatography (GC, Agilent 7890B) equipped with a HP-5 capillary column (30 m × 0.32 mm × 0.25 μm) using dodecane as internal standard. The products were identified by a GC–MS (Agilent 6890 N/5975). In order to test the catalytic reusability of Pd@MOF-253, after the reaction, the used catalyst was separated by filtration, washed with toluene and acetone, and dried in a vacuum drying oven at 80 °C for 12 h and then the recovered catalyst was directly used in the next reaction run (before the 5th re-cycling). When the catalytic activity decreased dramatically (such as 5th re-cycling), the H_2 reduction was then employed to activate catalyst for the next 6th and 7th re-cycling.

2.6. Characterization

The surface morphology of Pd@MOF-253 was imaged with a field emission scanning electron microscope (FESEM, S-4800, HITACHI) and a transmission electron microscope (TEM, JEOL-2100F). The high angle annular dark field (HAADF) and Energy-dispersive X-ray spectroscopy (EDS) elemental mapping images were obtained on an EDAX Genesis. The power X-ray diffraction (XRD) patterns were recorded on an X-ray diffractometer with Cu Kα radiation (D8 Advance, Bruker, $\lambda = 1.54059$ Å). The N_2 sorption isotherms were measured at 77 K on a Micromeritics ASAP 3020 using a liquid N_2 bath. Electron paramagnetic resonance (EPR) measurements were performed at the X-band using a JEOL FA 2000 spectrometer. 1H and 13C MAS NMR spectra were carried out in a 4 mm MAS probe on a Bruker AVANCE-III 400 spectrometer with a sample spinning rate of 10 kHz. ICP measurements were examined on inductively coupled plasma-atomic emission spectroscopy (ICP-AES, Prodigy7). Fourier transform infrared spectroscopy (FT-IR) spectra were obtained using a Bruker VerTex 80 v spectrometer. X-ray photoelectron spectroscopy (XPS) measurements were performed on a PHI Quantera II, (ULVAC-PHI, Japan) for chemical composition analysis, all binding energies were calibrated to the C1s peak at 284.8 eV. The measurement of H_2 Temperature-programmed desorption (TPD) was performed on an AutoChem II 2920 V5.02, and the procedure was displayed as follows: the sample (about 0.1 g) was first treated at 200 °C for 0.5 h in Ar. Then the reactor was cooled to 50 °C and exposed to 20% H_2/Ar for 30 min,

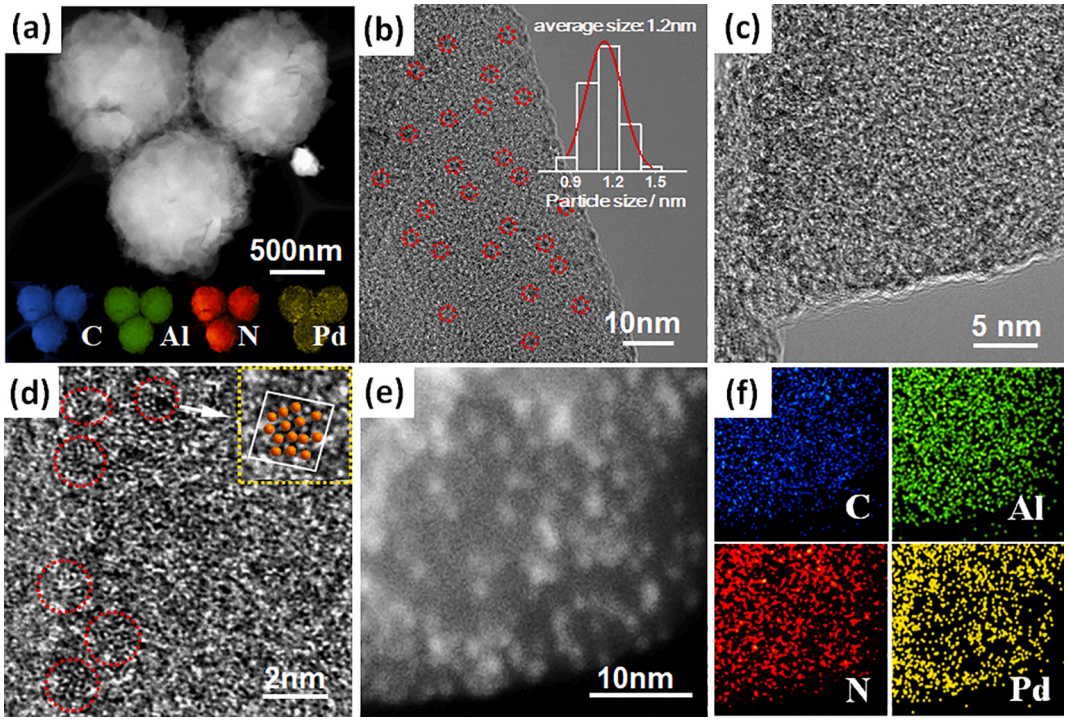

Fig. 1. (a) Low magnification STEM images, together with the corresponding EDX maps of 0.14 wt% Pd@MOF-253; (b) and (c) TEM images of 0.14 wt% Pd@MOF-253, the inset is the size distribution profile of the Pd clusters; (d) HRTEM of 0.14 wt% Pd@MOF-253 (the inset is Pd atomic position of the disordered phase with yellow sphere); (e) STEM images and (f) corresponding EDX element maps of 0.14 wt% Pd@MOF-253.

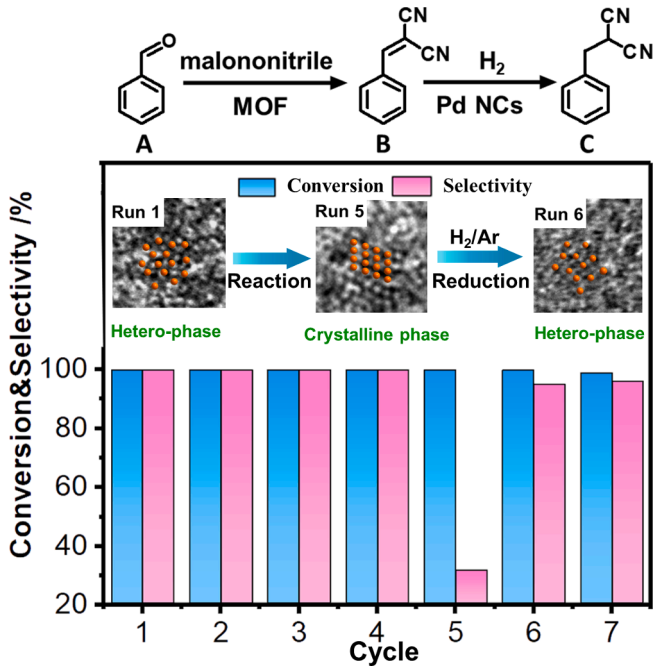

Fig. 2. Recycling tests of the 0.14 wt% Pd@MOF-253 in Knoevenagel condensation-hydrogenation of benzaldehydes with malononitrile. (Reaction conditions: first step, benzaldehyde (0.4 mmol), malononitrile (1.2 mmol), toluene (6 mL), and 20 mg of catalyst, room temperature, 12 h, stir at 600 rpm; second step, 0.12 MPa H_2, room temperature, 12 h, stir at 600 rpm). At the middle we show the structural changes of the Pd NP in the different runs. (The yellow sphere is the position of Pd phase).

and purged with Ar for 5 h at 50 °C in order to eliminate the physically adsorbed H_2. H_2-TPD was performed by ramping to 300 °C at 10 °C/min and H_2 in effluent was detected and recorded as a function of temperature on a TCD detector and a mass spectrometer simultaneously.

2.7. Density functional theory (DFT) calculations

The geometry of different size of Pd clusters and their coordinated complexes with bpydc ligands are fully optimized with B3LYP functional and 6–31 + g(d) basis set for C, N, H atoms and SDD pseudo potential using Gaussian 16 software [41]. Complexation energies between pyridine nitrogen and different types of Pd atoms are then calculated with the same method. The geometry of different size of Pd clusters and their coordinated complexes with bpydc ligands are fully optimized. Based on the fully optimized geometry of the Pd14 cluster, the adsorption energy of H_2 on disordered closed-packing, edge, and surface packing Pd atoms are calculated using the same method by freezing Pd14 cluster but having H atoms moving freely. Ab initio molecular dynamics simulations (AIMD) on the interaction of MOF-253 and cluster containing 20 Pd atoms are performed by using Vienna ab initio simulation package (VASP) under 500 K for 4 ps with a time step of 1 fs with NVT ensemble [42,43]. The ion–electron interactions were described by the projector augmented wave method. The generalized gradient approximation in the Perdew-Burke-Ernzerhof form and a cut-off energy of 300 eV for plane-wave basis set were adopted. The model of MOF-253 was built from the experimental crystal of DUT-5 by changing biphenyl linkers of DUT-5 to bipyridine. Both the structure and unit cells of MOF-253 model were then optimized. Supercells consisting of eight Al metals and the connected ligands and 20 Pd atoms, with the dimensions of a = 22.69800 Å, b = 13.21442 Å, c = 19.23980 Å, $\alpha = \beta = \gamma = 90°$, were built on the basis of the optimized MOF-253 crystal. The Brillouin zones were sampled by a Monkhorst-Pack k-point mesh with Gama k-point grid (1x1x1).

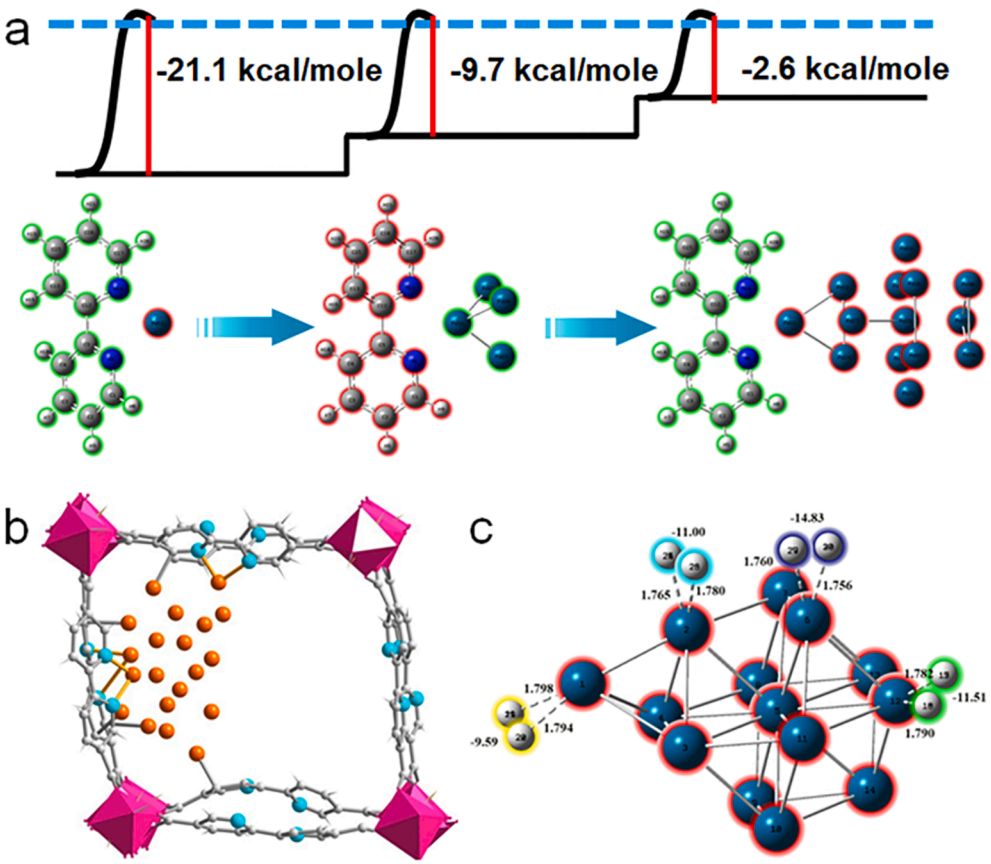

Fig. 3. (a) Calculated energies (kcal/mole) between pyridine nitrogen and different types of Pd assemblies; (b) the dynamics of MOF-253 containing 20 Pd atoms; (c) schematic presentation of the adsorption energies (in kcal/mol) of H_2 on different corners, edges and disordered cup of a Pd14 atoms with the Pd-H distances given in Å.

3. Results and discussion

The Al(OH)(bpydc) metal–organic framework (MOF-253; H_2bpydc = 2,2́-bipyridine-5,5́-dicarboxylic acid) is a material with excellent potential for serving as a catalytic support (Figure S1) [40,44]. The linkers, incorporating the 2,2́-bipyridine moiety, can efficiently coordinate metal ions and potentially anchor molecular catalytic species or even NPs. An ultra-low Pd loading (0.14 wt%) in MOF-253 (Pd@MOF-253) was purposefully targeted by a calculated impregnation, washing cycles and hydrogen reduction in order to reach very high dispersion of the Pd clusters. The powder XRD patterns of the as-synthesized Pd@MOF-253 (Figure S2) matches well with the simulated one for the non-loaded MOF-253, and no discernible peaks which could be attributed to Pd metal, are observed. All adsorption–desorption isotherms show a type I shape, which is characteristic of a microporous material (Figure S3). The BET surface area and pore volume of the Pd@MOF-253 material (Table S1) were reduced to 763 $m^2\ g^{-1}$ and 0.56 $cm^3\ g^{-1}$ in comparison with non-loaded MOF-253 (1395 $m^2\ g^{-1}$ and 0.84 $cm^3\ g^{-1}$).

The morphology, distribution, average particle size and structure of the Pd clusters (Fig. 1a, 1b and 1c) were examined by electron microscopy and energy dispersive X-ray analysis (EDX). High resolution transmission electron microscopy (HRTEM) images confirm the presence of Pd clusters with an average size of 1.2 nm and a remarkably narrow size distribution (inset in Fig. 1b). Fig. 1d shows HRTEM image of the Pd clusters. The disordered atoms arrangement (here we denoted as disordered phase) compared to the traditional orderly arranged Pd atoms (crystalline phase) are possibly caused by the anchor points, coordinated by the 2,2́-bipyridine. The role of the 2,2́-bipyridine could be assessed through the comparison of the NPs in Pd@MOF-253 and Pd@DUT-5 (using 4,4́-biphenyldicarboxylate (bpdc)) as support. The latter material is synthesized analogously to the former using a nearly isostructural DUT-5 support, which features biphenyl moieties instead of the chelating 2,2́-bipy moieties in MOF-253 (both exhibiting the same one dimensional pore with a size of 1.1 nm) (Figure S4). The average size of the Pd NPs in Pd@DUT-5 is 5.3 nm and hence they should be localized primarily on the surface of the support particles (Figure S5a). They are also more crystalline as confirmed by HRTEM (Figure S5b). EDX element mapping of a selected area of Pd@MOF-253 confirms the homogenous dispersion of all elements in the sample (Fig. 1e and 1f).

The successful establishment of Pd clusters within the framework of the MOF-253 further encouraged us to evaluate their catalytic activity towards heterogeneous catalysis. Considering the intrinsic Lewis basicity of Pd@MOF-253, the Knoevenagel condensation-hydrogenation reaction was chosen as a model reaction to evaluate the activity of the bifunctional Pd@MOF-253. It's worth noting that only the first step of reaction is taken place with traces of the final hydrogenated product being detected when the cascade-type reaction was performed with MOF-253, indicating that the Pd nanaocluster was the catalytic site for the second hydrogenation step (Table S2 and S3). Although the load of Pd is only 0.14 wt%, Pd@MOF-253 exhibits an excellent performance for the Knoevenagel condensation-hydrogenation reaction with complete conversion and > 99% selectivity towards benzylmalononitrile, even at room temperature, superior to some others reported Pd-based catalysts. The catalytic activity decreases apparently when the process goes on to the fifth cycle (only hydrogenation performance catalyzed by Pd clusters was significantly decreased while the Knoevenagel condensation was not affected). After the catalyst is reduced by 10% H_2/Ar at 200 °C for 3 h, the catalytic activity is surprisingly restored (see the results in the sixth and seventh cycle in Fig. 2). Very interestingly, the Pd nanostructure, shown in HRTEM (Figure 2 and S6), presents a dynamic

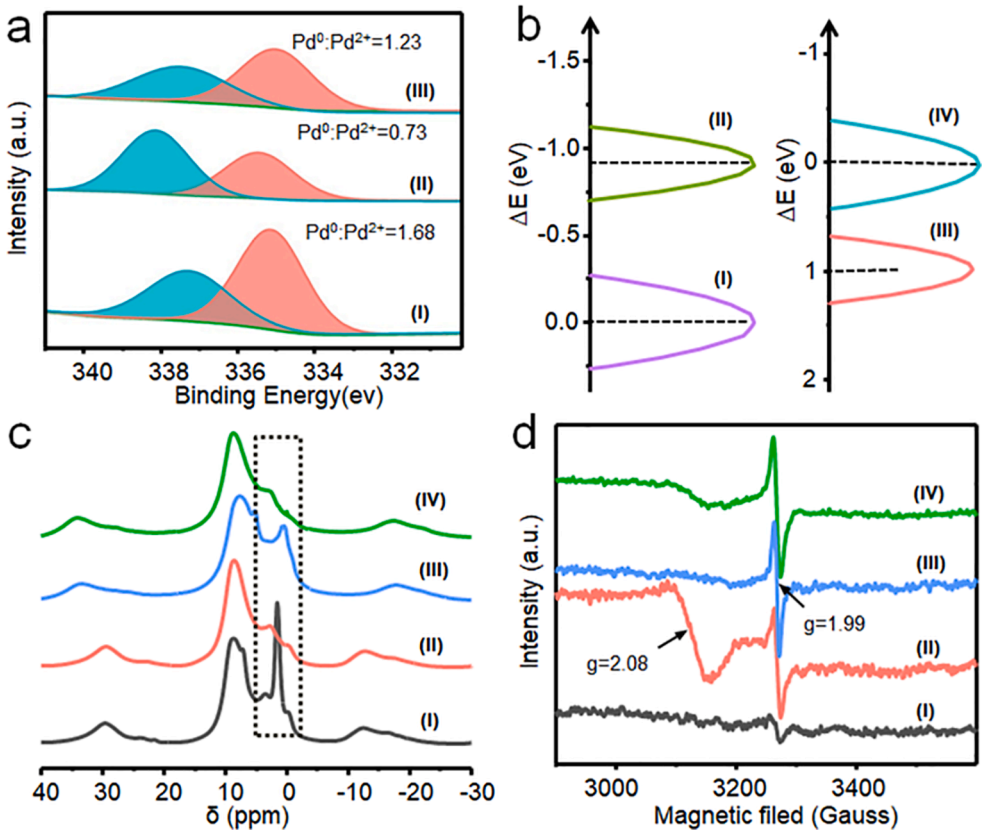

Fig. 4. (a) Pd $3d_{5/2}$ XPS spectra of 0.14 wt% Pd@MOF-253 (I), after cycle 5 times (II) and after H_2 reduction (III); (b) Pd $3d_{5/2}$ chemical shift of (I) Pd@DUT-5 and (II) Pd@MOF-253 (left), N 1 s chemical shift of (III) Pd@MOF-253 and (IV) MOF-253 (right); (c) 1H MAS NMR spectra and (d) EPR spectra for (I) MOF-253, (II) 0.14 wt% Pd@MOF-253, (III) after cycle 5 times and (IV) after H_2 reduction.

transition from clusters to crystalline NPs after 5 cycles and to re-generated clusters. A similar particle redispersion from large NPs to small-sized species on a carbon cloth in H_2 atmosphere has also been recently demonstrated [45], although this phenomenon was mostly discovered in the O_2 atmosphere [39,46].

In order to disclose the mechanism on the formation of Pd clusters, Density functional theory (DFT) calculations were carried out to study the interaction between pyridine nitrogen and Pd clusters. Calculated binding energies for interaction models between pyridinic nitrogen and different types of Pd atoms (a packing mode of 14 atoms, 3-coorperated cup atom as disordered closed-packing and 5-coorperated atom as edge and surface packing) are shown in Fig. 3. The average binding energy between single Pd and bipyridine in Pd1-bipyridine, Pd4-bipyridine and Pd14-bipyridine are about −21, −9.7 and −2.6 kcal/mole. This suggests that with an increasing number of Pd atoms, the average binding energy of Pd-bipyridine decreases rapidly, the coordinated effect of bipyridine reduces. Thus, the nucleation and growth of nearest Pd atoms within the MOF framework will be significantly influenced due to the much stronger host–guest interaction than distant Pd atoms, which tend to crystal with high order. Considering the microporous space of MOF-253, we theoretically designed a four layers cluster containing 14 Pd atoms to simulate the surface to bulk phase behavior of the Pd atoms; the first layered one Pd atom is the most active atom to connect with N, the second layer three Pd atoms are considered as surface phase atoms, the third layer seven Pd are bulk phase and the fourth layer three Pd are surface phase atoms. In this way, the disordered packing of the Pd clusters in the experimental results could be theoretically obtained. Furthermore, the growth process of the Pd cluster within the framework of MOF-253 was simulated using the Vienna ab initio simulation package (VASP) dynamic calculation (Fig. 3b, Figure S7). For random Pd atoms in the porous framework of MOF-253, their nucleation and growth process under the influence of pyridine nitrogen has been recorded. The relatively stable status of a Pd cluster supported on MOF-253 is shown in Fig. 3b. The host–guest interaction includes a relatively strong Pd-N coordination bond between Pd and pyridine nitrogen, d-π interactions between Pd and benzene rings, and Pd-H between Pd and Al-OH-Al. Generally, the relative H adsorption energy of Pd is critical to the desorption of H atoms from Pd and improves the catalytic activity of hydrogenation. We have calculated the energetics of the interaction of hydrogen with different types of Pd atoms within an isolated Pd14 cluster (Fig. 3c). The binding energy of H atoms on disordered 3-cooperated cup Pd is about 9.5 kcal/mol, which is much weaker than that on neighboring edge Pd atoms (11.0 kcal/mol) and inside surface Pd atoms (14.8 kcal/mol). These DFT results show how the Pd atoms nucleate, freely grow and easily form disordered packing Pd clusters when the number of atoms is below 15, in very good agreement with the experimental results. Moreover, the smaller adsorption energy of disordered Pd atoms than those of more ordered ones, indicates easier H_2 dissociation of disordered Pd atoms. The H_2 activation activity was further evaluated via the H_2-TPD measurement. As shown in Figure S8, the first peak at about 80 °C of Pd@MOF-253 and 100 °C of Pd@DUT-5 could be ascribed to the desorbed hydrogen that adsorbed on Pd species. Obviously, the much lower desorption temperature of H_2 for Pd@MOF-253 compared to Pd@DUT-5 confirmed that H_2 dissociation is easier on disordered Pd atoms than on Pd NPs, which might result in a high catalytic activity in hydrogenation reactions.

In order to further explore the mechanism of the regeneration of Pd and provide experimental evidence for the interaction between Pd and MOF-253, we performed a detailed characterization of the whole process (disordered packing, crystalline packing and re-disordered packing) by X-ray photoelectron spectroscopy (XPS), solid state nuclear magnetic resonance (NMR) spectroscopy and Electron paramagnetic resonance

Table 1
Knoevenagel condensation-hydrogenation of substituted benzaldehydes with malononitrile catalyzed by 0.14 wt% Pd@MOF-253.

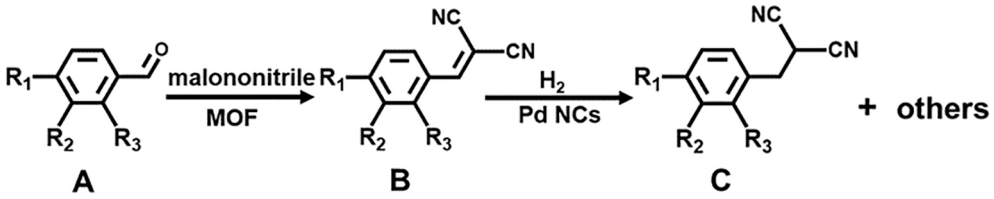

Entry	Substrates	Products	Conv.[%] A	Sel. [%] C	TOF(TON)/h^{-1}
1	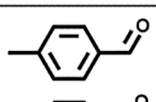	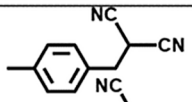	100	>99	30.4(548.0)
2	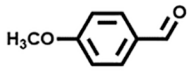	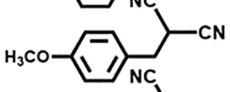	79	>99	21.8(393.0)
3	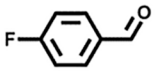	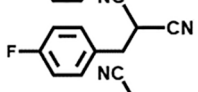	100	>99	30.8(545.7)
4	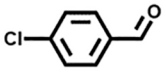	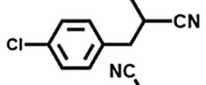	100	>99	36.8(481.8)
5	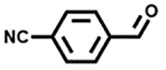	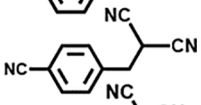	100	>99	28.7(516.5)
6	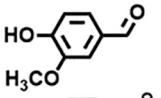	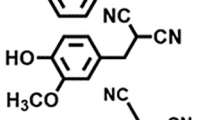	100	>99	24.7(445.2)
7	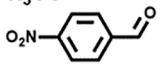	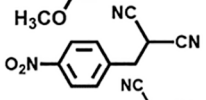	>99	51	12.7(228.6)
8	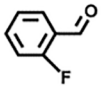	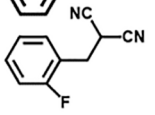	100	97	29.7(534.7)

(EPR). For XPS, the low binding energy doublets of Pd $3d_{5/2}$ and Pd $3d_{3/2}$ that appear at 335.15 and 336.06 eV for Pd@MOF-253 can be attributed to the formation of Pd0 species whereas the characteristic peaks of Pd $3d_{5/2}$ at 337.27 and 338 eV point to the possible presence of Pd^{2+} species (Figure S9). The Pd^0/Pd^{2+} ratio of starting cluster, 5-cycles larger-size nanocrystals and re-generated clusters is 1.68, 0.73 and 1.23 (Fig. 4a), indicating the catalytically active species Pd^0 can be dynamic, in good agreement with the catalytic results. The presence of the N1s binding energy peak at 398.7 eV for MOF-253 corresponds to the single-type symmetrical free pyridinic nitrogen (Figure S10). Compared to free pyridinic nitrogen in the MOF-253, the interactions of Pd and pyridinic N in a new N1s peak at 399.7 eV has shifted about 0.85 eV (Fig. 4b and S10b). Compared to Pd@DUT-5, a Pd^0 chemical shift of 0.9 eV is observed in Pd@MOF-253. These obvious shifts suggest that part of the pyridinic nitrogen atoms are coordinated by Pd species. The 1H MAS NMR spectrum exhibits three broad peaks at $\delta = 1.3$, 4.1 and 7.6 ppm which can be attributed to the Al-OH-Al bridging hydroxide protons, the water and the aromatic hydrogen, respectively (Fig. 4c) [47,48]. The bridging hydroxide protons of Al-OH-Al show an interesting difference of decreasing, increasing and decreasing, respectively, during the catalytic process. This not only proves that the H in Al-OH-Al can coordinate the Pd for the formation of clusters, but also indicates that the Pd in disordered status is very active and enable to bind with relatively stable H atoms. The 13C cross-polarization MAS NMR spectrum (Figure S11) confirms the protonated carboxy might partly contribute to the formation of Pd-H, observed by change of protonated forms ($\delta = 171$ ppm) and unchanged of deprotonated forms ($\delta = 173$ ppm). Meanwhile, a new peak around 685 cm^{-1} in the IR spectrum of Pd@MOF-253 appears and the peaks of carbonyl, Al-O-Al and Al-O display a slight shift (Figure S12). To obtain information about the active species of Pd@MOF-253, EPR spectra are recorded (Fig. 4d). The peak at $g = 1.99$ of all Pd@MOF-253 samples is due to Pd^0 clusters [49]. The peak at $g = 2.08$ is only observed in starting and regenerated Pd clusters, which is attributed to electro-accepted N. These results indicate that the proximal palladium atoms can donate electrons to the organic moiety of the secondary building unit in MOF-253. The strong host–guest interaction might be beneficial to the formation and regeneration of confined Pd clusters, activate the substrate molecule, and in return significantly decrease the activation energy during the catalytic process.

Encouraged by these results, we wanted to investigate the substrate applicability of the Pd@MOF-253 in a condensation-hydrogenation reaction by using a variety of substituted benzaldehydes. The results of the condensation-hydrogenation reactions are summarized in Table 1. Amazingly, even at room temperature and atmospheric pressure, almost all substituted benzaldehydes were completely converted to corresponding benzylmalononitriles with high yields, no matter whether benzaldehyde derivatives involved electron-donating groups (e.g., 2-OCH_3, 4-OCH_3 and 4-CH_3) or electron-withdrawing groups (e.g., 4-nitro, 4-F, 2-F and 4-Cl). Note that the relatively lower selectivity for 4-nitrobenzaldehyde is due to the simultaneous hydrogenation of -NO_2 and C = C groups in the second hydrogenation step. Other side products like 2-(4-aminobenzylidene)-malononitrile and 2-(4-aminobenzyl)-

malononitrile are also generated [18,50]. Besides, the heterogeneously catalytic nature has also been confirmed by the filtration experiments of Pd@MOF-253 in the hydrogenation reaction (Figure S13). Considering the ultralow Pd loading amount (0.14 wt%), our catalytic system represents a rare example of excellent performance in a one-pot condensation-hydrogenation reaction at atmospheric temperature and pressure, which is more efficient than most reported metal NPs@MOF catalysts [51,52]. The excellent catalytic performance especially under such ultralow loadings, we believe, benefits from the highly active confined Pd clusters.

4. Conclusion

In summary, ultrafine and highly dispersed Pd clusters (average size 1.2 nm) have been successfully obtained and regenerated after catalytic cycles by a strong metal-support interaction and confinement effects of the MOF-253. Experiments and theoretical computations have been conducted to study the strong host–guest interaction between Pd and the MOF support, leading to a high catalytic activity and dynamic structure of the Pd clusters. It is believed that this new design idea will open a new frontier on the preparation of diversified supported noble metal catalysts with both excellent catalytic efficiency and stability.

Declaration of Competing Interest

The authors declare that they have no known competing financial interests or personal relationships that could have appeared to influence the work reported in this paper.

Acknowledgements

We acknowledge a joint NSFC-DFG project (NSFC grant 51861135313, DFG JA466/39-1), National Natural Science Foundation of China (21706199, U1662134), ISTCP (2015DFE52870), National Key R&D Program of China (2017YFC1103800), NSFHP (2016CFA033, 2017CFA006, 2017CFB487), Jilin Province Science and Technology Development Plan (20180101208JC), Fundamental Research Funds for the Central Universities (FRFCU, 19lgzd16), Rapid Response Bilateral Collaborative Funding of the Sino-German Center for Research Promotion (C-0046), International Science & Technology Cooperation Program of China (2015DFE52870), Guangdong Province International Scientific and Technological Cooperation Projects (2020A0505100036).

Appendix A. Supplementary data

Supplementary data to this article can be found online at https://doi.org/10.1016/j.cej.2021.132128.

References

[1] F. A. Lewis, Academic Press: New York (1967).
[2] G. C. Bond, Academic Press: New York (1962).
[3] H. Nakatsuji, M. Hada, J. Am. Chem. Soc. 107 (1985) 8264–8266.
[4] H. Zhang, M. Jin, Y. Xiong, B. Lim, Y. Xia, Acc. Chem. Res. 46 (2013) 1783.
[5] B.D. Adams, A. Chen, Mater. Today 14 (2011) 282.
[6] A. Chen, C. Ostrom, Chem. Rev. 115 (2015) 11999.
[7] Q. Yang, Q. Xu, S.H. Yu, H.L. Jiang, Angew. Chem. Int. Ed. 55 (2016) 3685–3689.
[8] I. Saldan, Y. Semenyuk, I. Marchuk, O, J. Mater. Sci. 50 (2015) 2337.
[9] X. Chen, K. Shen, D. Ding, J. Chen, T. Fan, R. Wu, Y. Li, ACS Catal. 8 (2018) 10641–10648.
[10] S. Ma, D. Yuan, J.S. Chang, H.C. Zhou, Inorg. Chem. 48 (2009) 5398–5402.
[11] S. Yuan, L. Feng, K. Wang, J. Pang, M. Bosch, C. Lollar, Y. Sun, J. Qin, X. Yang, P. Zhang, Q. Wang, L. Zou, Y. Zhang, L. Zhang, Y. Fang, J. Li, H.C. Zho, Adv. Mater. 30 (2018), e1704303.
[12] G. Huang, Q. Yang, Q. Xu, S.H. Yu, H.L. Jiang, Angew. Chem. Int. Ed. 55 (2016) 7379–7383.
[13] Y. Liu, X.-C. Ma, G.-G. Chang, S.-C. Ke, T. Xia, Z.-Y. Hu, X.-Y. Yang, J. Colloid Interface Sci. 557 (2019) 207–215.
[14] L. Chen, H. Chen, R. Luque, Y. Li, Chem. Sci. 5 (2014) 3708–3714.
[15] X.-F. Yang, A. Wang, B. Qiao, J. Li, J. Liu, T. Zhang, Acc. Chem. Res. 46 (2013) 1740.
[16] N. Yang, H. Cheng, X. Liu, Q. Yun, Y. Chen, B. Li, B. Chen, Z. Zhang, X. Chen, Q. Lu, J. Huang, Y. Huang, Y. Zong, Y. Yang, L. Gu, H. Zhang, Adv. Mater. 30 (2018) 1803234.
[17] S. Lu, Y. Hu, S. Wan, R. McCaffrey, Y. Jin, H. Gu, W. Zhang, J. Am. Chem. Soc. 139 (2017) 17082.
[18] M. Zhao, K. Deng, L. He, Y. Liu, G. Li, H. Zhao, Z. Tang, J. Am. Chem. Soc. 136 (2014) 1738.
[19] H. Kou, J. Lu, Y. Li, Adv. Mater. 26 (2014) 5518.
[20] R.A. Dalla Betta, R.C. McCuney, J.W. Sprys, Ind. Eng. Chem. Prod. Res. Dev. 15 (1976) 169–172.
[21] J. Wang, F. Xu, H. Jin, Y. Chen, Y. Wang, Adv. Mater. 29 (2017) 1605838.
[22] L. Zhu, X.Q. Liu, H.L. Jiang, L.B. Sun, Chem. Rev. 117 (2017) 8129–8176.
[23] A. Aijaz, T. Akita, N. Tsumori, Q. Xu, J. Am. Chem. Soc. 135 (2013) 9–16356.
[24] D.-D. Zu, L. Lu, X.-Q. Liu, D.-Y. Zhang, L.-B. Sun, J. Phys. Chem. C 118 (2014) 19910–19917.
[25] X. Li, Z. Guo, C. Xiao, T.W. Goh, D. Tesfagaber, W. Huang, ACS Catal. 4 (2014) 3490–3497.
[26] H. Leiske, G. Lietz, H. Spindler, J. Volter, J. Catal. 81 (1983) 8–16.
[27] M.H. Groothaert, P.J. Smeets, B.F. Sels, P.A. Jacobs, Schoonheydt, R. A, J. Am. Chem. Soc. 127 (2005) 1394–1395.
[28] H. Birgersson, L. Eriksson, M. Boutonnet, S.G. Jaras, Appl. Catal. B 54 (2004) 193–200.
[29] B. Aguila, Q. Sun, X. Wang, E. O'Rourke, A.M. Al-Enizi, A. Nafady, S. Ma, Angew. Chem. Int. Ed. 57 (2018) 10107–10111.
[30] W.Y. Gao, Y. Chen, Y. Niu, K. Williams, L. Cash, P.J. Perez, L. Wojtas, J. Cai, Y.-S. Chen, S. Ma, Angew. Chem. Int. Ed. 53 (2014) 2615–2619.
[31] Y. Nishihata, J. Mizuki, T. Akao, H. Tanaka, M. Uenishi, M. Kimura, T. Okamoto, N. Hamada, Nature 418 (2002) 164.
[32] Y. Lu, Xl. Liu, L. He, YX. Zhang, ZY. Hu, G. Tian, X. Cheng, SM. Wu, YZ. Li, XH. Yang, LY. Wang, JW. Liu, Janiak. Christoph, GG. Chang, WH. Li, Tendeloo. Gustaaf Van, X-Y. Yang, BL. Su, Nano Lett., 20 (5) (2020)3122-3129.
[33] ST. Xiao, SM. Wu, Y. Dong, JW. Liu, LY. Wang, L. Wu, YX. Zhang, G. Tian, Janiak. Christoph, Shalom. Menny, YT. Wang, YZ. Li, RK. Jia, Bahnemanni. Detlef W, XY. Yang, Chem Eng J, 400 (2020) 125909.
[34] M.A. Newton, C. Belver-Coldeira, A. Martínez-Arias, M. Fernández-García, Nat. Mater. 6 (2007) 528.
[35] S.-M. Wu, X.-Y. Yang, C. Janiak, Angew. Chem. Int. Ed. 131 (2019) 12468–12482.
[36] Y. Lu, X. Cheng, G. Tian, H. Zhao, L. He, J. Hu, S.-M. Wu, Y. Dong, G.-G. Chang, S. Lenaerts, S. Siffert, G. Van Tendeloo, Z.-F. Li, L.-L. Xu, X.-Y. Yang, B.-L. Su, Nano Energy 47 (2018) 8–17.
[37] S.-M. Wu, X.-L. Liu, X.-L. Lian, G. Tian, C. Janiak, Y.-X. Zhang, Y. Lu, H.-Z. Yu, J. Hu, H. Wei, H. Zhao, G.-G. Chang, G. Tendeloo, L.-Y. Wang, X.-Y. Yang, B.-L. Su, Adv. Mater. 30 (2018) 1802173.
[38] G.-G. Chang, X.-C. Ma, Y.-X. Zhang, L.-Y. Wang, G. Tian, J.-W. Liu, J. Wu, Z.-Y. Hu, X.-Y. Yang, B. Chen, Adv. Mater. (2019) 1904969.
[39] M. Moliner, J.E. Gabay, C.E. Kliewer, R.T. Carr, J. Guzman, G.L. Casty, P. Serna, A. Corma, J. Am. Chem. Soc. 138 (2016) 15743.
[40] E.D. Bloch, D. Britt, C. Lee, C.J. Doonan, F.J. Uribe-Romo, H. Furukawa, J.R. Long, O.M. Yaghi, J. Am. Chem. Soc. 132 (2010) 14382.
[41] Gaussian 16, Revision A.03, Frisch, M. J.; Trucks, G. W.; Schlegel, H. B.; Gaussian, Inc., Wallingford CT, (2016).
[42] G. Kresse, J. Furthmüller, Efficient iterative schemes for ab initio total-energy calculations using a plane-wave basis set, Phys. Rev. B 54 (1996) 11169.
[43] G. Kresse, D. Joubert, From ultrasoft pseudopotentials to the projector augmented-wave method, Phys. Rev. B 59 (1999) 1758–1775.
[44] I. Senkovska, F. Hoffmann, M. Fröba, J. Getzschmann, W. Böhlmann, S. Kaskel, Microporous Mesoporous Mater. 122 (2009) 93.
[45] J.M. Chen, H.Y. Wang, Z. Wang, S.J. Mao, J. Yu, Y. Wang, Y. Wang, ACS Catal. 9 (2019) 5302–5307.
[46] L.C. Liu, D.N. Zakharov, R. Arenal, P. Concepcion, E.A. Stach, A. Corma, Nat. Commun. 9 (2018) 574.
[47] T. Loiseau, C. Serre, C. Huguenard, G. Fink, F. Taulelle, M. Henry, T. Bataille, G. Férey, Chem-Eur J. 10 (2004) 1373–1382.
[48] J. Gascon, U. Aktay, M.D. Hernandez-Alonso, G.P.M. van Klink, F.J. Kapteijn, Catal. 261 (2009) 75.
[49] A.S. Roy, J. Mondal, B. Banerjee, P. Mondal, A. Bhaumik, S.M. Islam, Appl. Catal. A-Gen. 469 (2014) 320–327.
[50] N. Tirelli, A. Altomare, R. Solaro, F. Ciardelli, U. Meier, C. Bosshard, P. Günter, J. Prakt. Chem. 340 (1998) 122–128.
[51] E. Verde-Sesto, E. Merino, E. Rangel-Rangel, A. Corma, M. Iglesias, F. Sánchez, ACS Sustainable Chem. Eng. 4 (2016) 1078–1084.
[52] X. Li, B. Zhang, Y. Fang, W. Sun, Z. Qi, Y. Pei, S. Qi, P. Yuan, X. Luan, T.W. Goh, W. Huang, Chem-Eur J. 23 (2017) 4266–4270.